Journal of Materials Chemistry A

Accepted Manuscript

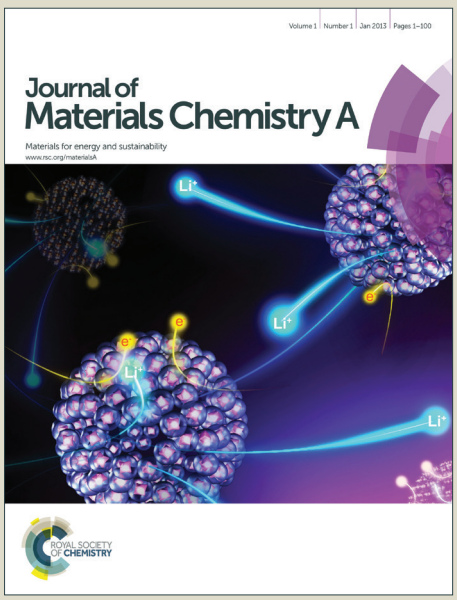

ROYAL SOCIETY OF CHEMISTRY

www.rsc.org/materialsA

Cite this: DOI: 10.1039/c0xx00000x

www.rsc.org/xxxxxx

ARTICLE TYPE

Construction of 3D-rGO network-wrapping architecture in $Yb_yCo_4Sb_{12}$/rGO composite for enhancing thermoelectric performance

Peng-an Zong[a,e], Xihong Chen[b], Yanwu Zhu[c], Ziwei Liu[d], Yi Zeng[d] and Lidong Chen*[a]

Received (in XXX, XXX) Xth XXXXXXXXX 20XX, Accepted Xth XXXXXXXXX 20XX
DOI: 10.1039/b000000x

Nanostructures and nano-composites have been shown effective to depress lattice thermal conductivity and improve the performance of thermoelectric materials. However, ZT enhancement by nano-particle dispersion is limited only in restricted level due to the difficulty to increase the particle contents while maintaining uniform and narrow size distribution. In the present work, $Yb_yCo_4Sb_{12}$-based nano-composites with reduced graphene oxide (rGO) layers of several nanometers intercalated on the grain boundary matrix forming a 3D network has been prepared through a simple in-situ reduction approach using graphene oxide (GO) as precursors. The 3D-rGO network wrapping architecture dramatically reduced lattice thermal conductivity due to enhanced interparticle and intraparticle phonon scattering effects, and simultaneously enhanced Seebeck coefficient due to energy filtering effect of the grain boundary semiconductive rGO layer in nanometer thickness. The maximum ZT value of 1.51 was achieved in $Yb_{0.27}Co_4Sb_{12}$/rGO (0.72 vol%) composite at 850K, outperforming all single-filled skutterudites and their nanocomposites ever reported.

1. INTRODUCTION

Thermoelectric effects enable a direct conversion between thermal energy and electricity providing a promising solution for global sustainable energy. The efficiency of a thermoelectric device is basically determined by a dimensionless figure of merit (ZT) of the thermoelectric materials, quantified by $ZT = (S^2\sigma T)/\kappa$, ($\sigma$, S, T and κ are the Seebeck coefficient, electrical conductivity, absolute temperature and thermal conductivity, respectively). The thermal conductivity κ is comprised of two components: (i) the electron part κ_E, contributed from heat transportation by carriers; (ii) the phonon part κ_L, contributed from heat transportation by phonons travelling through lattice.[1,2] In the past decade, effective strategies have been used to tune the thermal and electrical transport,[3-8] and many novel thermoelectric materials with enhanced ZTs have been reported.[9-16] Among them, $CoSb_3$–based filled skutterudites (SKD) are one of the most promising materials for power generation applications in mediate temperature range. In $CoSb_3$–based skutterudites with cage structure, filling one or multiple kinds of guest atoms (alkali metals, alkaline earth, rare earth, and some other ions) into the intrinsic Sb-icosahedron cage has been shown effective to suppress the lattice thermal conductivity with a minimized influence on electrical transport. Typically, the maximum ZT value has reached over 1.7 in the multiple-filled skutterudites, in which two or three kinds of elements with different resonant frequencies were filled into the Sb-icosahedron cage to scatter phonons in a broad range of frequencies, with optimized filling contents for optimizing charge concentration.[3]

Compared to multiple-filled skutterudites, single-filled skutterudites also receive great expectation in mass production for industrial applications, because their simple composition leads to better controllability of the process and potential for scaling-up and cost-down in industrialized fabrication. Further reducing lattice thermal conductivity is the most challenging but most effective for raising ZT values of single-filled skutterudites. Constructing nano-structure or nano-composite is one of the most commonly used strategies for strengthening the phonon scattering.[2, 11-16] So far, lots of skutterudites-based or filled skutterudites-based nano composites have been synthesized by dispersing different nano-particles, such as $CoSb_3/C_{60}$[11] and $CoSb_3/ZrO_2$[12] fabricated by mechanical mixing, $Ba_{0.22}Co_4Sb_{12}/TiO_2$ [13] by solution dispersion, $Yb_xCo_4Sb_{12}/Yb_2O_3$,[14] $Yb_xCo_4Sb_{12}/Sb$[15] and $Yb_xCo_4Sb_{12}/GaSb$[16] by in-situ reaction. Particularly, for the typical n-type filled skutterudite $Yb_xCo_4Sb_{12}$, which is one of the candidates for device applications, ZT_{max} values have been continuously enhanced by dispersing different nanoparticles from less than 1.2 (pure $Yb_xCo_4Sb_{12}$) to ~1.3 ($Yb_xCo_4Sb_{12}/Yb_2O_3$[14]) and ~1.4 ($Yb_xCo_4Sb_{12}/GaSb$[16]). In these nano-particle dispersed systems, both the interfaces between matrix and nano-particles and the nano-particles themselves act

as the objectives to scatter phonons.[13-16] However, the depression of lattice thermal conductivity is still limited in such nano particle-dispersed systems, because the total amount of the nano-particles and the interfaces are limited in a relatively low level. Further more, the narrow size distribution of the nano-particles is difficult to be obtained in bulk materials due to the agglomeration of nano-particles. Additionally, in oxide particles dispersed systems, the electron scattering is also not negligible, which usually damages the electrical transport.

Recently, an ideal 3D network wrapping structure (or core-shell nanocomposites) has been proposed theoretically for strengthening the phonon scattering and holding the promise of *ZT*-plus.[17,18] According to this model, when the secondary phase disperses as a nanoscale shell layer on the grains of matrix phase (core), the heat-carrying phonons would be much more effectively scattered than the particle dispersion system, because of the enhanced interparticle boundary scattering and intraparticle boundary scattering with increased interface amount. However, it is of great challenge to realize such a 3D network architecture in a bulk material. In addition, the 3D network wrapping nanocomposite demands more strict requirement on the electrical property of the introduced wrapping phase so that it can scatter phonons but maintain a good electron transport, because all the matrix grains would be wrapped by the dispersion phase. A high electrical conductivity with a suitable band gap matching with the matrix would be required because an extra potential at the boundaries would be expected to realize energy-filtering effect[16] in such 3D-wrapping structure. In order to satisfy these demands, we propose to use reduced graphene (rGO) as the wrapping phase because the band gap can be tuned by the reduction degree (the oxygen ratio in rGO).[20,21] We designed a $Yb_{0.27}Co_4Sb_{12}$-based composite with rGO nanolayers intercalating on the grain boundary forming continuous 3D network. However, a big challenge arises for constructing such rGO 3D-network architecture in SKD/rGO composites, because of the easy agglomeration[11-15] due to poor dispersity of rGO. The graphene oxide (GO) is known having better dispersity in appropriate agent or water solutions. In previous reports, $CoSb_3$/graphene[22] and PbTe/graphene[23] were synthesized by a wet chemical method, where the matrix-$CoSb_3$ and PbTe were fabricated by a solvothermal method and the GO was concurrently reduced by $NaBH_4$. However, the graphene needs to get thinner and better its distribution to form an interconnected network to further depress thermal conductivity, because the solvothermal method may lead to rapid agglomeration of graphene during reduction of graphene, and the wet-chemically prepared matrix may restrict the optimization of thermoelectric performance to some extent by deteriorating electrical properties due to relatively low purity of the matrix. We developed a simple in-situ reduction approach to realize the 3D-rGO network wrapping structure using the GO as the precursor. In this simple process, the GO was dispersed into the solid-state-melting-method made $Yb_yCo_4Sb_{12}$ skutterudite (SKD) powder to fabricate SKD/GO mixture, and then the powder mixture compact was densified using spark plasma sintering, whereby the GO was reduced to rGO. The rGO layers as thick as ~3-5 nm are homogeneously distributed on grain boundaries. The obtained SKD/rGO composite with well-designed 3D network structure exhibited extremely low lattice thermal conductivity and relatively high power factor (particularly high Seebeck coefficient) as compared with single-filled skutterudites and their composites. An enhancement of ~ 30% in *ZT* value was achieved in the wide temperature range between 300 to 850 K with a maximum *ZT* value of 1.51 at 850K.

2. EXPERIMENTAL SECTION

2.1 Synthesis and Sample Preparation

$Yb_{0.27}Co_4Sb_{12}$ (SKD) powder was fabricated by a solid state melting method.[13] Improved Hummers method [21,24] was applied to synthesize GO from purified natural graphite (SP-1, Bay Carbon). Then 1.5g fine SKD powder was dispersed in 200 ml deionized water, then dropwise added 0.05 mg/ml GO water suspension solution, followed by the ultrasonic treatment for 30 min. The mixture was then subjected to vacuum filtering, drying at 450 K in Ar-5 vol % H_2 gas flow for 4 h, regrinding into fine powder. The SKD/GO mixture powder compacts were then sintered by spark plasma sintering in a graphite die in vacuum at 900 K for 10 minutes under an axial pressure of 60 MPa, yielding fully densified bulk disk-shaped samples, containing various rGO content (y = 0, 0.72, 1.8, 3.6 vol %) in SKD. The synthesis process was schematically shown in Fig. 1.

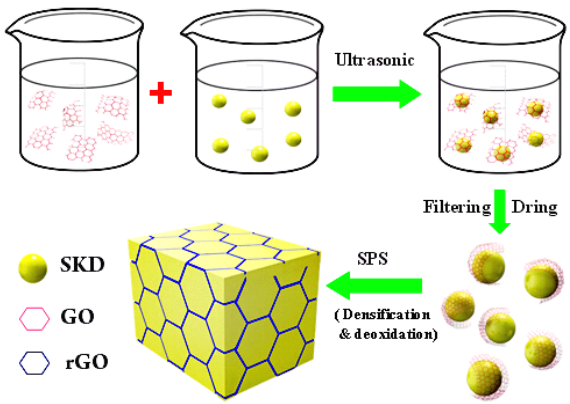

Fig. 1 Three-dimensional schematic showing synthesis procedures of 3D-rGO network wrapping architecture

2.2 Structure Analysis

The powder constituent phase was determined with X-ray diffractometry (CuKa, Rigaku, Rint 2000) equipped with Cu Kα radiation (λ = 1.5418 Å). The morphology and microstructure were investigated with field emission scanning electron microscopy (FESEM, Hitachi S-4800). Transmission electron microscopy (TEM) investigations were carried out on a JEM 2010 microscope. Traditional standard TEM specimen preparation processes were used to prepare the thin TEM specimens, consisting of cutting, grinding, mechanical polishing and low-voltage (1.5 V) Ar-ion milling on a liquid nitrogen cooling stage. The thin TEM specimens were nitrogen plasma cleaned by for 30s, then used for scanning transmission electron microscopy (STEM) investigation (FEI Magellan 400) with an accelerating voltage of 30 kV. To evaluate the reduction degree of GO after SPS process, X-ray photoelectron spectroscopy (XPS) was carried out on pure GO compact treated by SPS under the same conditions as the SKD/GO samples. Both the as-prepared

GO and the pure GO compact after SPS treatment were ion etched at 1 kV and 1 μA for 10 seconds on an area of 1 mm × 1 mm with EX05 argon ion gun. The XPS analysis was conducted on a Thermo Scientific ESCALAB 250Xi with a monochromated Al X-ray source ($h\nu$ = 1486.6 eV), operating at a beam energy of 15 kV, a beam current of 10 mA and an incident angle of 58°, while an electron flood gun was used for charge compensation.

2.3 Thermal Property Measurements

The SPS-sintered pellets were grinding and polishing into disk-shaped samples with 10 mm diameter and ~2 mm thickness for thermal diffusivity measurement. A thin graphite layer was coated on two sides of the disc samples to impede emissivity from the samples. The total thermal conductivity (κ) was calculated by $\kappa = \rho C p \lambda$, where ρ is density of the bulk samples determined by Archimedes method (METTLER TOLEDO AB104-L), Cp is the specific heat determined by differential scanning calorimetry (DSC 404C, Netzsch, Germany). λ is the thermal diffusivity coefficient from 300 to 850 K measured on Netzsch LFA427 by Laser flash method with an applied laser voltage of 450 V and a pulse width of 0.5 ms. The thermal diffusivity data were analyzed using a Cape-Lehman method with pulse correction.

2.4 Electrical Property Measurements

Rectangular bars with dimensions of ~ 8 mm × 2 mm × 2mm were obtained by cutting in the radial direction of the SPS-sintered disc samples and subsequently used for simultaneous measurement of electrical conductivity (σ) and Seebeck coefficient (S) from room temperature to 850 K under a helium atmosphere with a vacuum degree of -0.09 MPa on the ULVAC-RIKO ZEM-3 device. Rectangular bars with dimension of ~ 5 mm × 2 mm × 1 mm were cut from the sintered pellet for low temperature electrical property characterization. PPMS-Quantum Design was utilized to determine the electrical conductivity (σ) from 3 to 300K with a four-probe configuration and Hall coefficient (R_H) with a five-probe configuration under a magnetic field of -5T to 5T. Measurements on both positive and negative magnetic field directions were carried out to minimize the magneto-resistance contributions as well as the voltage probe misalignment effects. The carrier concentration (n) was calculated from $R_H = 1/ne$, and the mobility (μ_H) from $\mu_H = \sigma/ne$, where e is the electron charge.

3. RESULTS AND DISCUSSIONS

3.1 Structure of $Yb_{0.27}Co_4Sb_{12}$/rGO composite

Constructing a 3D-rGO network structure intercalated in skutterudite matrix is the emphasis of this work. In order to evaluate the effectiveness of SPS process on the reduction of GO, pure GO compact was treated by SPS under the same condition as sintering the SKD/GO compact and then X-ray photoelectron spectroscopy (XPS) analysis was conducted on the GO samples before and after SPS treatment. High resolution XPS spectra of C 1s are shown in Fig. 2a and 2b. The asymmetric C 1s peak can be fitted with peaks with binding energy at 284.6, 285.6, 286.9, and 288.6 eV, assigned to sp^2-C 1s, C-OH, C-O-C, and O=C-O bonds, respectively. It is clear that the peak of graphitic sp^2-C 1s at ~284.5 eV was narrowed, while the signals of hydroxyl (C-O) ~285.6 eV and C-O-C ~286.9 eV become weaker and the peak of O=C-O at ~288.6 eV disappeared after SPS. All these observations deliver evidences that GO has been partially reduced by SPS treatment. It was reported that the reduction or partial deoxidization of oxides used to take place during SPS process under a vacuum in a graphite die due to the strong reducing atmosphere around the particles induced at high temperature[25-27] and surface deoxidation effect[28,29] by electrical discharge. In the present experiment, the graphene oxides are considered being partially deoxidized by the accelerated thermal reduction in SPS process.

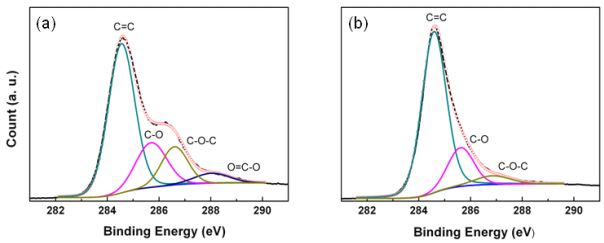

Fig. 2 Deconvoluted XPS spectra of (a) as-prepared GO and (b) rGO after SPS treatment.

The oxygen contents were also estimated from the XPS spectra and the O/C atomic ratio were determined. The O/C ratio depressed to a much lower value of 1/17.7 by SPS treatment from 1/2.2 for the as-prepared GO. Since most of the carbon atoms in GO are sp^3 hybridized, after chemical or thermal reduction, the size and numbers of sp^2 domains would increase and a percolated sp^2 network would grow on the basis of sp^3-hybridized area, earmarking an insulator to semiconductor transition with decreased work function and band gap values.[30] The work function and band gap in rGO with different reduction degree are reported being dependent on the O/C ratio.[31,32] According to the theoretical relationship between the O/C ratio and work function proposed by Pritank et al.,[31] values of the work function are estimated as ~ 5.3 for the as-prepared GO and ~ 4.7eV for rGO after SPS, respectively. The values of band gap are estimated as ~ 2.8 and ~0.5 eV for GO before SPS and rGO after SPS, respectively, according to Huang's relationship.[32] The reduction degree of the in-situ sintered rGO under the same SPS condition is regarded to be the same or similar. The dependence of composite performance on the reduction degree requires further study, for which new synthesis techniques should be developed.

Fig. 3a shows the typical TEM photograph of the GO-wrapped SKD particle obtained by water solution suspending and filtering/drying process. GO owns an ultrahigh specific surface energy,[18] and thus can readily wrap the suspending particles with excellent dispersion. Consequently, the SKD particles are well enclosed by ultrathin GO layers. The SEM photograph of the fractured surface of sintered SKD/rGO (0.72 vol%) (Fig. 3b) also shows that the rGO nano-layers are embedded on grain boundaries, as marked by the white arrows. A low-magnification TEM image (Fig. 3c) reveals that the matrix particles are distinctly and equably surrounded by rGO nano-layers as well. The high-magnification TEM image of SKD/rGO (0.72 vol%) sample (Fig. 3d) further demonstrates that the particles are separated by rGO layers of ~3-5 nm, occasionally covering the phonon MFP of filled skutterudite (~3 nm).[33,34] Comparatively, it

is found that the average thickness of the rGO layers on the SKD grain boundary grows from ~3-5 nm for 0.72 vol% 3D-rGO to ~6-8 nm for 1.8 vol% 3D-rGO sample, and ~10-12 nm for 3.6 vol% 3D-rGO sample (See Supporting Information (SI), Fig. S2a,b). The growing thickness may deteriorate electron transport and the detailed influence on the thermoelectric transport will be discussed later.

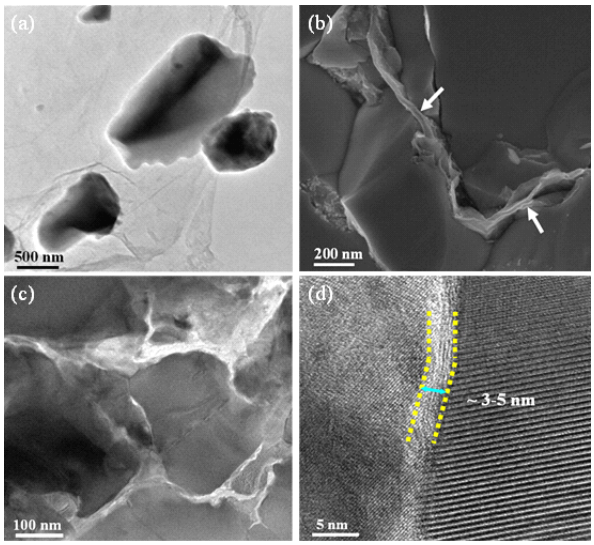

Fig. 3 Morphology and structure of $Yb_yCo_4Sb_{12}$/rGO Composite: (a) TEM image of GO-wrapped $Yb_{0.27}Co_4Sb_{12}$ obtained by solution dispersion and filtering/drying process, (b) SEM image of fractured surface of sintered SKD/rGO surface showing rGO embedding on boundaries, (c) Low-magnification TEM image showing network wrapping architecture of rGO nanolayers and (d) High-magnification TEM image showing rGO nanolayer of ~3-5 nm thick for 0.72 vol% 3D-rGO sample.

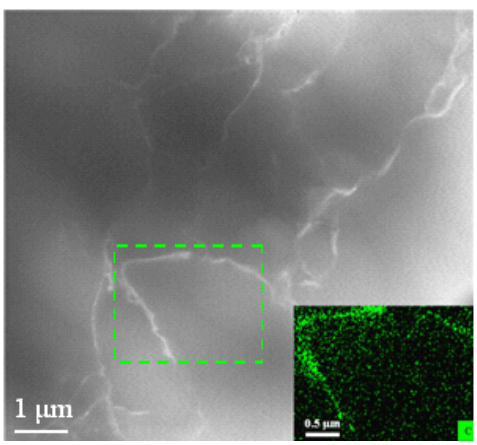

Fig. 4 HAADF-STEM image of $Yb_{0.27}Co_4Sb_{12}$/1.8 vol% 3D-rGO wrapping sample. Inset: Local energy spectrum analysis for carbon .

To make a visual display of the 3D-rGO network wrapping architecture, high angle annular dark-field imaging (HAADF) was conducted as shown in Fig. 4. The interconnected rGO construct a network embedding on grain boundaries, which is bright white in Fig. 4. The EDS analysis in the inset reconfirms the existence of rGO on grain boundaries. From the above XPS analysis and TEM/SEM/STEM observation, it can be concluded that, a 3D-rGO network wrapping architecture embedded in the SKD polycrystalline bulk is experimentally established through the in-situ reduction approach.

3.2 Thermal Transport of $Yb_{0.27}Co_4Sb_{12}$/rGO Composite

Fig. 5a shows the total thermal conductivity (κ) as a function of temperature for SKD/rGO samples with different rGO content (y). The κ of the matrix sample ($Yb_{0.27}Co_4Sb_{12}$) is consistent with those of the $Yb_yCo_4Sb_{12}$ skutterudite reported previously.[14,16,38] The κ values of the obtained 3D-rGO samples decrease significantly with y increment, attributing to the decline of both κ_E (discussed later) and κ_L, where κ_L was computed by subtracting κ_E via Wiedemann-Franz law from the total κ. Fig. 5b shows the κ_L as a function of temperature for SKD/rGO samples. κ_L of 0.72 vol% 3D-rGO sample demonstrates the lowest value in the temperature range from 300-850K. The lowest value of κ_L = 0.57 W m^{-1} K^{-1} (750K), approaching the theoretical limit of the minimum value (0.3 W m^{-1} K^{-1}),[14] is considered to tremendously contribute to the depression of total thermal conductivity. The rGO content (y) dependency of κ and κ_L, typically at 300 and 850 K (inset in Fig. 5b) for 3D-rGO wrapping and PD (particle dispersion) samples further prove the significance of κ_L depression especially at 0.72 vol%-rGO by the 3D-rGO wrapping structure. When the rGO content further increases, the κ_L undergoes a gentle rise from 0.72 vol% to 3.6 vol%, and surpasses the matrix's at 3.6 vol%. It is considered to be caused by the volume effect of rGO dispersion phase, because the volume effect gradually becomes dominant than the interparticle and intraparticle boundary scattering effects when the content of rGO dispersion phase (which possesses higher thermal conductivity) increases.[16] The HRTEM observation (See Fig. S2b) indicated that the increasing rGO content leads to a thicker network layer to ~ 10-12 nm for 3.6 vol% 3D-rGO sample .

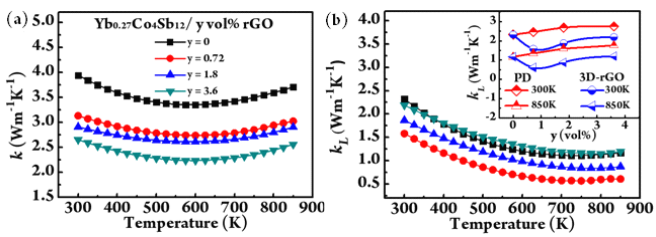

Fig. 5 (a) The thermal conductivity, and (b) lattice thermal conductivity as a function of temperature for $Yb_{0.27}Co_4Sb_{12}$/y vol% 3D-rGO (y = 0, 0.72, 1.8, 3.6) wrapping samples. Inset: rGO content (y) dependence of κ_L at 300K, 850K for 3D-rGO wrapping samples and particle dispersion (PD) samples obtained by direct mixing and sintering process as comparison, respectively.

3.3 Electrical Transport of $Yb_{0.27}Co_4Sb_{12}$/rGO Composite

Fig. 6a shows the temperature-dependent electrical conductivity (σ) of the obtained 3D-rGO wrapping samples with different rGO content (y). For the matrix SKD sample (0 vol%-rGO), σ values at room temperature and 850K are 2.69 × 10^5 S m^{-1} and 1.49 × 10^5 S m^{-1}, respectively. The 0.72 vol% 3D-rGO sample shows almost the same values and same temperature dependence with the matrix SKD sample, i.e., 2.58 × 10^5 S m^{-1} at room temperature and 1.42 × 10^5 S m^{-1} at 850K. As illustrated in Fig. 3d, the 0.72

vol% 3D-rGO sample has an rGO network layer with thickness of ~ 3-5 nm, which can strongly scatter phonons but give little influence on σ. rGO was reported showing p-type semiconduction above room temperature,[20,30] but a certain amount of the sp^2-conjuncted hexagonal graphene lattice is disrupted by C-O bonds which deteriorates the electron transport. In present case, when y is larger than 1.8 vol%, the thickness of the network layer soon becomes above 10 nm. As the thickness of rGO layer increases, volume effects[16] for both thermal and electrical properties would gradually become dominant, leading to the deterioration of σ. The temperature dependence of σ undergoes a change from a degenerating semiconducting behavior to an intrinsic one (dσ/dT changes from negative to positive). It remains a challenge to further characterize the electrical and thermal transport properties of the nano rGO layers embedding on the matrix grain boundaries to reveal in depth the influence of the electrical and thermal transport properties of the rGO on the composite performance.

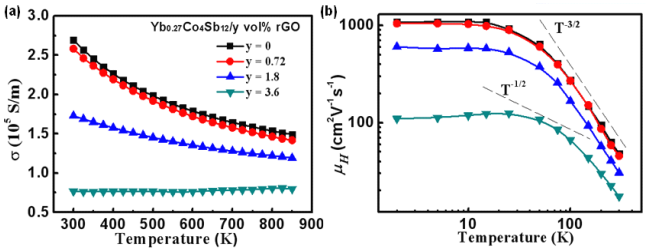

Fig. 6 (a) Electrical conductivity and (b) electron mobility as a function of temperature for $Yb_{0.27}Co_4Sb_{12}$/y vol% rGO (y = 0, 0.72, 1.8, 3.6) 3D wrapping samples.

The electron transport properties of 3D-rGO wrapping samples are further investigated by measurement of the electron mobility (μ_H), shown in Figure 6b. For the 3D-rGO wrapping samples, when y = 0, the relationship of $\mu_H \propto T^{\alpha}$ (α = -3/2) is observed near room temperature, manifesting a dominant mechanism of acoustic phonon scattering that agrees with reported data of pure filled skutterudites. The curve of 0.72 vol% and 1.8 vol% 3D-rGO samples resemble that of y = 0 (α = -3/2), indicating that the same scattering mechanism dominates the transport in the samples with rGO content less than 1.8 vol%. However, for the 3.6 vol% sample, the scattering parameter was observed between -3/2 and -1/2 near room temperature, indicating that a mixed scattering mechanism dominates the transport in this sample.

Fig. 7 shows the Seebeck coefficients and power factors as the function of temperature and/or carrier concentration for the obtained 3D-rGO wrapping samples with different rGO content (y). Electrons are the major carriers in $Yb_{0.27}Co_4Sb_{12}$/rGO samples showing negative S. All 3D-rGO wrapping samples have higher $|S|$ compared to that of the matrix. Owing to Fermi level gap between the matrix and rGO, the band may bend away from the interface, whereby an extra potential at the boundaries thus would be produced. The energy barrier produced by the phase interface between the matrix and rGO would scatter electrons with low energy and enhance the S, called energy-filtering effect.[33,34] Given a compound of a fixed band structure, the $|S|$ only depends on carrier density, and decrease with increasing n (carrier concentration). As shown in Fig. 7a, the $|S|$ values of all 3D-rGO wrapping samples increased with increasing rGO content, which does not only stem from the contribution of decreased carrier concentration. Hall measurement indicates that y = 0.72 sample (n = 3.42 × 10^{20} cm^{-3}, S = -127.1 μV K^{-1}) has almost the same n value but a higher $|S|$ compared to y = 0 sample (n = 3.56 × $10^{20}$$cm^{-3}$, S = -121.1 μV K^{-1}). Fig. 7b shows n-dependent S for $Yb_xCo_4Sb_{12}$,[38] nanoparticle-dispersed $Yb_xCo_4Sb_{12}$[13,14] and $Yb_{0.27}Co_4Sb_{12}$/rGO (present work). All S values for $Yb_xCo_4Sb_{12}$ follow a linear curve of $|S|$ *vs.* n (logarithmic coordinate). However, the S values of some nanoparticle-dispersed systems ($Yb_yCo_4Sb_{12}$/GaSb) and the present samples deviates from the line, indicating a remarkably enhanced $|S|$ under a given carrier concentration. As it is proved, energy-filtering effect is considered to depend on the phase-interface area between 'host' and 'guest'.[39] rGO network architecture provides abundant phase-interface for energy filtering to enhance $|S|$. The enhancement of $|S|$ is comparable to Xiong's $Yb_yCo_4Sb_{12}$/GaSb[16] composite. With slightly decrease of σ but enhanced $|S|$, y = 0.72 sample exhibits slightly-improved power factors as shown in Fig. 7c. Especially, σS^2 of y = 0.72 rGO sample reaches 41.4 μW cm^{-1} K^{-2} at room temperature and 54.2 μW cm^{-1} K^{-2} at 800K, while σS^2 of the matrix is 39.4 μW cm^{-1} K^{-2} at room temperature and 52.4 μW cm^{-1} K^{-2} at 800K, indicating that the increase of $|S|$ weighs over the decrease of σ.

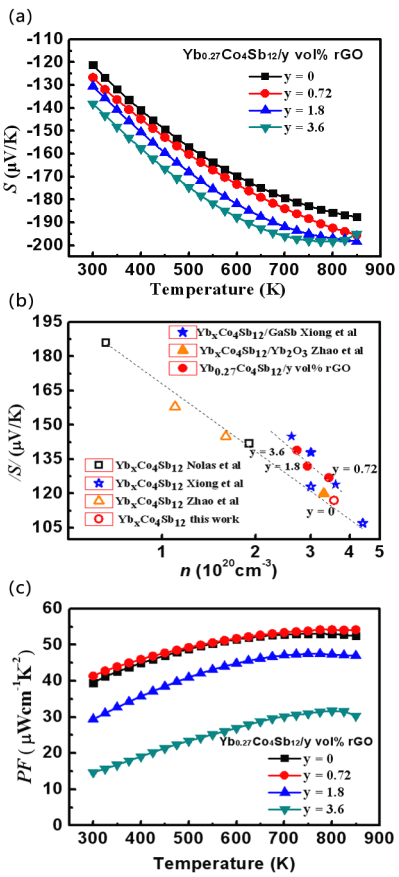

Fig. 7 (a) The Seebeck coefficient as a function of temperature, (b) carrier concentration dependent Seebeck coefficient in logarithmic coordinate, and (c) power factor as a function of temperature for $Yb_{0.27}Co_4Sb_{12}$/y vol % rGO (y = 0, 0.72, 1.8, 3.6) 3D network wrapping samples.

3.4 Thermoelectric Figure of Merit

Temperature dependencies of *ZT* for all $Yb_{0.27}Co_4Sb_{12}$/rGO samples with 3D-rGO wrapping structure are shown in Fig. 8. The inset shows y-dependence of *ZT* for comparison between 3D-rGO wrapping samples and particle-dispersed (PD) samples at 850K. *ZT* values of 3D-rGO wrapping samples show a remarkable enhancement when $y \leq 1.8$, then drop down with y increment, and tends to merge with that of PD samples when $y \geq 3.6$. This result demonstrates that 3D-rGO wrapping architecture can effectively depress thermal conductivity while maintain or even raise electrical transport (power factor). Optimized *ZT* is achieved with a proper rGO content ($y \leq 1.8$). But when rGO content (y) increases to 3.6, the rGO layer becomes enough thick (See Fig. S2) so that the volume effect begins to be dominant. *ZT* value thus tends to resemble that of y = 3.6 PD sample. If we define a $\Delta(ZT)/ZT$ as the *ZT* increase rate from y = 0 sample (ZT_m) to y = 0.72, 1.8, 3.6 samples (ZT_c), calculated by $\Delta(ZT)/ZT = (ZT_c - ZT_m)/ZT_m \times 100\%$, a prominent ZT increase rate of 32% (at 300K), 26% (at 850K) is achieved for 0.72 vol% 3D-rGO sample. ZT value reaches a peak of 1.51 at 850K for 0.72 vol% 3D-rGO sample. $\Delta(ZT)/ZT$ of 1.8 vol% 3D-rGO sample is relatively low, but positive and grows up to 11% (ZT = 1.34, at 850K). Considering the whole temperature range from 300-850K, the average *ZT* value ZT_{ave} of 0.72 vol% 3D-rGO sample reached 1.13. We can expect an optimal thermoelectric conversion efficiency η_{opt}[40] of 16.3%, outclassing results of single filled skutterudite and their composites previously reported.

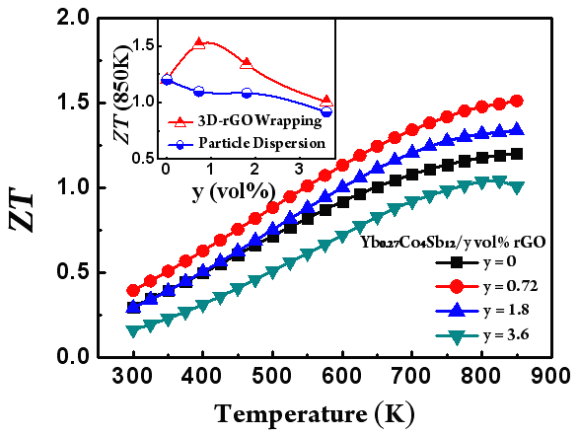

Fig. 8 Temperature-dependent *ZT* for $Yb_{0.27}Co_4Sb_{12}$/y vol% rGO (y = 0, 0.72, 1.8, 3.6) 3D wrapping samples from 300-850K. Inset: comparison of y-dependent *ZT* between 3D-rGO wrapping samples and particle dispersion samples at 850K.

Conclusions

$Yb_yCo_4Sb_{12}$-based composites with rGO intercalated on the $Yb_yCo_4Sb_{12}$ grain boundary forming 3D network wrapping architecture have been synthesized by in-situ reduction process. When the rGO content is less than 1.8 vol%, the thickness of the rGO layer on the grain boundary of $Yb_yCo_4Sb_{12}$ matrix is less than 10 nm, and lattice thermal conductivity is greatly decreased while the power factor maintains slight change resulting in great enhancement in *ZT*. The 3D-rGO network-wrapping architecture using GO as precursor goes beyond nano particles dispersion system and takes advantage of phonon constrain of wider wavelengths. Giant depression of κ_L by ~ 34-58% and then a *ZT* value up to 1.51 at 850K is achieved. This result outperforms all reported single-filled skutterudites and their nano-composites, which earmarks 3D-rGO network wrapping architecture to be a competitive route to state-of-the-art thermoelectric materials.

Acknowledgments

This work was supported by the National Natural Science Foundation of China (No. 51121064 and No.11179013) and 973 Program of National Basic Research Program of China (No. 2013CB632501). Y. Zhu appreciates the support from Natural Science Foundation of China (No. 51322204) and the Fundamental Research Funds for the Central Universities (No. WK2060140014). P. Zong also thanks Dr. Lin Tianquan for kind help in XPS spectra analysis.

Notes and references

[a] *State Key Laboratory of High Performance Ceramics and Superfine Microstructure, Shanghai Institute of Ceramics, Chinese Academy of Sciences, Shanghai 200050, China. Fax: +86 21 52413122; Tel: +86 21 52414804; E-mail: chenlidong@mail.sic.ac.cn; zongpengan@student. sic. ac.cn*

[b] *CAS Key Laboratory of Materials for Energy Conversion, Shanghai Institute of Ceramics, Chinese Academy of Sciences, Shanghai 200050, China. Fax: +86 21 52413122; Tel:+86 21 52412520; E-mail: xhchen @mail.sic.ac.cn*

[c] *Department of Materials Science and Engineering, University of Science and Technology of China & Collaborative Innovation Center of Chemistry for Energy Materials (2011-iChEM), Hefei 230026, China; Fax:+86 551 63601696; Tel:+86 551 6360767; E-mail: zhuyanwu@ ustc. edu.cn*

[d] *Analysis and Testing Center for Inorganic Materials, Shanghai Institute of Ceramics, Chinese Academy of Sciences, Shanghai 200050, China. Fax: +86 21 52413903; Tel: +86 21 52413108; E-mail: zengyi@mail.sic.ac.cn; ziweiliu@mail.sic. ac.cn*

[e] *University of Chinese Academy of Sciences, Beijing 100049, China*

† Electronic Supplementary Information (ESI) available: SEM images of 1.8 vol% 3D-rGO sample and 1.8 vol% particle dispersion sample respectively; TEM images of SKD/y vol% 3D-rGO samples (y = 1.8, 3.6); Thermoelectric properties of SKD/y vol% particle dispersion samples (y = 0, 0.72, 1.8, 3.6). See DOI: 10.1039/b000000x/

1 K. Biswas, J. Q. He, I. D. Blum, C. I. Wu, T. P. Hogan, D. N. Seidman,V. P. Dravid and M. G. Kanatzidis, *Nature*, 2012, **489**, 414.
2 G. J. Snyder and E. S. Toberer, *Nat. Mater.*, 2008, **7**, 105.
3 X. Shi, J. Yang, R. J. Salvador, M. F. Chi, Y. J. Cho, H. Wang, S. Q. Bai, J. H. Yang, W. Q. Zhang and L. D. Chen, *J. Am. Chem. Soc.*, 2011, **133**, 7837.
4 Pei, Y. Z.; Shi, X. Y.; Lalonde, A.; Wang, H.; Chen, L. D.; Snyder, G. J. *Nature*, **2011**, 473, 66.
5 H. L. Liu, X. Shi, F. F. Xu, L. L. Zhang, W. Q.Zhang, L. D. Chen, Q. Li, C. Uher, T. Day, G. J. Snyder, *Nat. Mater.*, 2012, **11**, 422.
6 L. D. Zhao, S. Q. Hao, S. H. Lo, C, I. Wu, X. Y. Zhou, Y. Lee, H. Li, K. Biswas, T. P. Hogan, C. Uher, C. Wolverton, V. P. Dravid, M. G. Kanatzidis, *J. Am. Chem. Soc.*, 2013, **135**, 7364.
7 Y. L. Pei, H. J. Wu, D. Wu, F. S. Zheng, J. Q. He, *J. Am. Chem. Soc.*, 2014, **136**, 13902.
8 L. D. Zhao, S. H. Lo, Y. Zhang, H. Sun, G. Tan, C. Uher, C. Wolverton, V. P. Dravid, M. G. Kanatzidis, *Nature*, 2014, **508**, 373.
9 R. J. Korkosz, T. C. Chasapis, S. Lo, J. W. Doak, Y. J. Kim, C. I. Wu, E. Hatzikraniotis, T. P. Hogan, D. N. Seidman, C. Wolverton, V. P. Dravid, M. G. Kanatzidis, *J. Am. Chem. Soc.*, 2014, **136**, 3225.

10 L. D. Zhao, H. J. Wu, S. Q. Hao, C. I. Wu, X. Y. Zhou, K. Biswas, J. Q. He, T. P. Hogan, C. Uher, C. Wolverton, V. P. Dravid, M. G. Kanatzidis, *Energy Environ. Sci.*, 2013, **6**, 3346.
11 X. Shi, L. D. Chen, J. Yang, G. P. Meisner, *Appl. Phys. Lett.*, 2004, **84**, 2301.
12 Z. He, C. Stiewe, D. Platzek, G. Karpinski, E. Müller, S. H. Li, M. Toprak, M. Muhammed, *J. Appl. Phys.*, 2007, **101**, 043707.
13 Z. Xiong, X. H. Chen, X. Y. Zhao, S. Q. Bai, X. Y. Huang, L. D. Chen, *Solid State Sci.*, 2009, **11**, 1612.
14 X. Y. Zhao, X. Shi, L. D. Chen, W. Zhang, S. Q. Bai, Y. Z. Pei, X. Y. Li, T. Goto, *Appl. Phys. Lett.*, 2006, **89**, 092121.
15 H. Li, X. Tang, X. Su, Q. Zhang, *Appl. Phys. Lett.*, 2008, **92**, 202114.
16 Z. Xiong, X. H. Chen, X. Y. Huang, S. Q. Bai, L. D. Chen, *Acta Mater.*, 2010, **58**, 3995.
17 S. J. Poon, A. S. Petersen, D. Wu, *Appl. Phys. Lett.*, 2013, **102**, 173110.
18 Y. W. Zhu, S. Murali, W. Cai, X. Li, J. W. Suk, J. Potts, *Adv. Mater.*, 2010, **22**, 3906.
19 L. D. Chen, Z. Xiong, S. Q. Bai, *J. Inorg. Mater.*, 2010, **25**, 561.
20 N. Xiao, X. C. Dong, L. Song, D. Y. Liu, Y. Y. Tay, X. S. Wu, L. J. Li, Y. Zhao, T. Yu, H. Zhang, W. Huang, H. H. Hng, P. M. Ajayan, Q. Y. Yan, *ACS Nano*, 2011, **5**, 2749.
21 S. Stankovich, R. D. Piner, X. Q. Chen, N. Q. Wu, S. T. Nguyen, R. S. Ruoff, *J. Mater. Chem.*, 2006, **16**, 155.
22 B. Feng, J. Xie, G. S. Cao, T. J. Zhu, X. B. Zhao, *J. Mater. Chem.* A, 2013, **1**, 13111
23 J. D. Dong, W. Liu, H, Li, X. L. Su, X. F. Tang, C. Uher, *J. Mater. Chem.* A, 2013, **1**, 12503
24 W. S. Hummers, R. E. Offeman, *J. Am. Chem. Soc.*, 1958, **80**, 1339.
25 S. Ran, J. Vleugels, S. Huang, K. Vanmeensel, D. H. A.Blank, L. Winnubst, *J. Eur. Ceram. Soc.*, 2010, **30**, 899.
26 S. Yoon, J. Dornseiffer, Y. Xiong, D. Grüner, Z. Shen, S. Iwaya, C. Pithan, R. Waser, *J. Eur. Ceram. Soc.*, 2011, **31**, 773.
27 N. Mahmed, O. Heczko, R. Maki, O. Söderberg, E. Haimi, S. Hannula, *J. Eur. Ceram. Soc.*, 2012, **32**, 2981.
28 N. Toyofuku, T. Kuramoto, T. Imai, M. Ohyanagi, Z. A. Munir, *J. Mater. Sci.*, 2012, **47**, 2201.
29 X. P. Li, M. Yan, H. Imai, K. Kondoh, G. B. Schaffer, M. Qian, *J. Non-Cryst. Solids*, 2013, **375**, 95.
30 C. Punckt, F. Muckel, S. Wolff, I. A. Aksay, C. A. Chavarin, G. Bacher, W. Mertin, *Appl. Phys. Lett.*, 2013, **102**, 023114.
31 V. K. Pritank, B. Marco, C. G. Jefferey, *ACS Nano*, 2013, **7**, 1642.
32 H. M. Huang, Z. B. Li, J. C. She, W. L. Wang, *J. Appl. Phys.*, 2012, **111**, 054317.
33 T. Caillat, A. Borshchevsky, J. P. Fleurial, *J. Appl. Phys.*, 1996, **80**, 4442.
34 J. Yang, W. Zhang, S. Q. Bai, Z. Mei, L. D. Chen, *Appl. Phys. Lett.*, 2007, **90**, 192111.
35 J. P. Heremans, V. Jovovic, E. S. Toberer, A. Saramat, K. Kurosaki, A. Charoenphakdee, S. Yamanaka, G. J. Snyder, *Science*, 2008, **321**, 554.
36 S. V. Faleev, F. Léonard, *Phys. Rev. B.*, 2008, **77**, 214304.
37 D. H. Sim, Q. Yan, D. Liu, X. Dong, N. Xiao, S. Li, Y. Zhao, L. J. Li, Q. Y. Yan, H. H. Hng, *J. Phys. Chem. C.*, 2011, **115**, 1780.
38 G. S. Nolas, M. Kaeser, I. R. Littleton, T. M. Tritt, *Appl. Phys. Lett.*, 2000**,** **77**, 1855.
39 S. Katsuyama, M. Watanabe, M. Kuroki, T. Maehata and M. Ito, *J. Appl. Phys.*, 2003, **93**, 2758.
40 B. Poudel, Q. Hao, Y. Ma, Y. C. Lan, A. Mininnich, B. Yu, X. Yan, D. Z. Wang, A. Muto, D. Vashaee, X. Y. Chen, J. M. Liu, M. Dresselhaus, G. Chen and Z. F. Ren, *Science*, 2008, **320**, 634.